-RESEARCH PAPER-

International Journal of Mining and Geo-Engineering

IJMGE

IJMGE 60-2 (2026) 171-178

DOI: 10.22059/IJMGE.2026.387231.595213

A mechanical earth model with velocity matching algorithm for predicting shear wave velocity using offset well data from an Iranian oilfield

Abolfazl Abdollahipour [a,*]

[a] *School of Mining Engineering, College of Engineering, University of Tehran, Tehran, Iran.*

Article History:

Received: 22 December 2024.

Revised: 17 December 2025.

Accepted: 03 May 2026.

ABSTRACT

A Mechanical Earth Model (MEM) provides the geomechanical properties required for wellbore stability, well completion, hydraulic fracturing, and mud weight design. This study presents a one-dimensional MEM for a vertical well in a Berriasian–Santonian oilfield in southwest Iran. Shear wave velocity was not measured in the target well and was instead predicted from an adjacent offset well using a velocity matching algorithm that aligns compressional delay times. The novelty of this approach lies in systematically reconstructing missing shear data to enable MEM construction under data-limited conditions. The MEM includes pore pressure, in situ stress fields, and rock mechanical properties along the well path. Static laboratory tests were correlated with dynamic log data to generate continuous rock strength profiles. Using these inputs, a mud weight window was computed and compared with drilling operations. The predicted window showed good agreement with observed breakouts in FMI logs and daily drilling reports. Stability analysis across several intervals indicated that the most stable wellbore trajectory varies with depth due to changes in stress regime and mechanical properties. The method assumes sonic similarity between adjacent wells and is limited by the small number of core samples and incomplete log coverage. Nevertheless, the study demonstrates that velocity matching from an offset well is a practical tool for MEM development, improving wellbore stability prediction and trajectory optimization.

Keywords: *Mechanical earth model; Elastic properties; In-situ stress; Wellbore stability; Mud weight window.*

1. Introduction

A Mechanical Earth Model (MEM) is a crucial tool in petroleum engineering, providing a quantitative description of rock mechanical properties and in-situ stresses in the subsurface. 1D MEM is the most common type, typically constructed using well-log data, direct pressure measurements, and rock strength parameters [1]. It provides profiles of in-situ stresses and mechanical properties of geological formations along a wellbore.

Construction of a mechanical earth model is a perquisite to any geomechanical analysis. The MEM uses log data, core data, pressure, and stress measurements to build a reliable distribution of geomechanical properties of a reservoir. The MEM provides the required geomechanical properties for many engineering analyses including wellbores stability [2], completions and hydraulic fracturing design [3, 4], selecting safe mud window, selection of casing points, and optimizing the number of casing strings [4–7]. A reasonably accurate MEM may considerably optimize the time and cost by predicting some of the problems that can occur during drilling and production operations. Predicting shear wave velocity is extremely important for Mechanical Earth Models (MEM). Shear wave velocity characterizes subsurface formations and influences geomechanical behavior [8, 9]. Accurate predictions are essential for assessing elastic properties and wellbore stability. Shear wave velocity is also crucial for modeling seismic wave propagation and interpreting seismic data [10–12]. Reliable predictions enhance MEM accuracy and enable more precise simulations of coupled processes. This contributes to better decision-making in oil and gas reservoir exploration and production.

In recent years, data-driven and ensemble-based approaches have been employed to predict elastic parameters in gas reservoirs by integrating multiple predictive models to improve robustness and uncertainty handling [13]. While such methods demonstrate the capability of indirect elastic property estimation in data-limited settings, they generally do not explicitly enforce stress–strain consistency and geomechanical constraints inherent to Mechanical Earth Models.

A one-dimensional MEM consists of in situ stress field and pore pressure along with geomechanical properties of a well path. Pore pressure may be determined from leak-off and extended leak-off tests (LOT & XLOT), drill stem tests (DST), and modular formation dynamic tester (MDT). Abnormal pore pressures may occur if pore fluid cannot escape impermeable formations in case of rapid compaction [14, 15]. Many relations have been developed to predict pore pressure gradient from well logs. These relations use velocity, resistivity, and porosity data [16–22]. The dynamic properties may be determined from density logs and sonic logs. Many relations have also been proposed to determine static elastic properties from dynamic counterparts. However, these relations are only applicable to a range of rocks and are even limited to certain formations. There are various proposed relations to convert dynamic Young's modulus to static Young's modulus for Limestone, sandstone, shale etc [23–29]. Another set of relations estimates UCS from static Young's modulus [30–34]. However, the best estimation of geomechanical properties for a certain formation must be derived from a correlation between that formations log data and laboratory tests on cores.

* Corresponding author. *E-mail address:* Abdollahipour@ut.ac.ir (A. Abdollahipour).

In this study, a mechanical earth model is developed for an oilfield in Southwest of Iran. In situ stresses are determined using a leak-off test. The orientations of in situ stresses are determined from FMI and breakouts orientations in the well. The required relations are derived from correlations between log data and laboratory rock mechanic test results on the available cores. The MEM is verified with drilling reports and calipers log observations. A stability analysis is also provided, showing the optimized well path for the widest mud weight window.

2. Geology and description of the oilfield

The oilfield is situated in the southwestern region of Iran. It spans a length of 20 kilometers and has a width of 2.5 kilometers, stretching in a north-south direction. Its total area is approximately 52 km2. The well XX1 was drilled through multiple formations, namely Gurpi, Ilam, Sarvak, Kazhdumi, Dariyan, Gadvan, and Fahlian. Among these, the Sarvak, Kazdumi sandstone, Gadvan, and limestone intervals of the Fahliyan formations are the primary producing horizons in this field. These formations represent a range of ages, spanning from the early to late Cretaceous epoch. They primarily consist of Dolomite, Calcite, Clay, and Quartz.

To construct the MEM, data from two wells were collected. The data obtained from well XX1 included wireline logs, mud weight, drilling reports, and 12 drill stem tests (DSTs). Additionally, data from an adjacent well XX2, including a leak-off test, compressional delay time (DT), and shear delay time (DTS), were also provided. The wireline logs in well XX1 provided information on thickness, lithology, and formation tops. They also included caliper, gamma ray, formation density, and compressional delay time (DT). The main inputs for computing the elastic properties of the formations are the sonic and density log data.

3. In situ stress field

In situ stresses play a determining role in wellbore stability evaluations. The vertical stress and two horizontal stresses are usually the principal stresses in a field (in absence of tectonic forces). Several methods have been developed to determine these stresses. Jaeger and Cook developed a method to determine principal stresses in a critically oriented fault at frictional limit [35]. Zoback et al. developed stress polygon concept to constrain stress magnitudes [36, 37]. The principal stresses usually (in absence of significant folding or salt domes) consist of the total vertical stress Sv the total minimum horizontal stress Sh and the total maximum horizontal stress SH. A main component in calculating the horizontal stresses is pore pressure. Therefore, pore pressure should be determined before stress calculations.

3.1. Pore pressure

Pore pressure Pp is an important component in an MEM, and critical to the calculation of horizontal stresses and wellbore stability analysis. Pore pressure in well XX1 is calculated based on the results of 12 DST tests in this well. An average pore pressure gradient resulting in the same pore pressures as those of DST results in the respective TVDs was used to calculate a continuous pore pressure profile throughout the well depth. As shown in "Pressures" track of Figure 1, pore pressure (shown with solid red line in Figure 1) is almost equal to hydrostatic pressure up to Fahlian formation. This formation is known for its high abnormal pressure. Therefore, drilling crew always drills through this formation with caution, using a high mud pressure (shown with solid black line in Figure 1) to prevent kick and blowout.

3.2. Effect of Ore Hardness on Exhaust Fan Power and Mill Pressure

The vertical stress is usually considered to be solely due to the weight of the overburden. Using continuous formation density, one may calculate the vertical stress Sv by integrating formation bulk density ρb from surface to TVD using the following equation:

$$S_v = \int_0^z \rho_b(z).g.dz \quad (1)$$

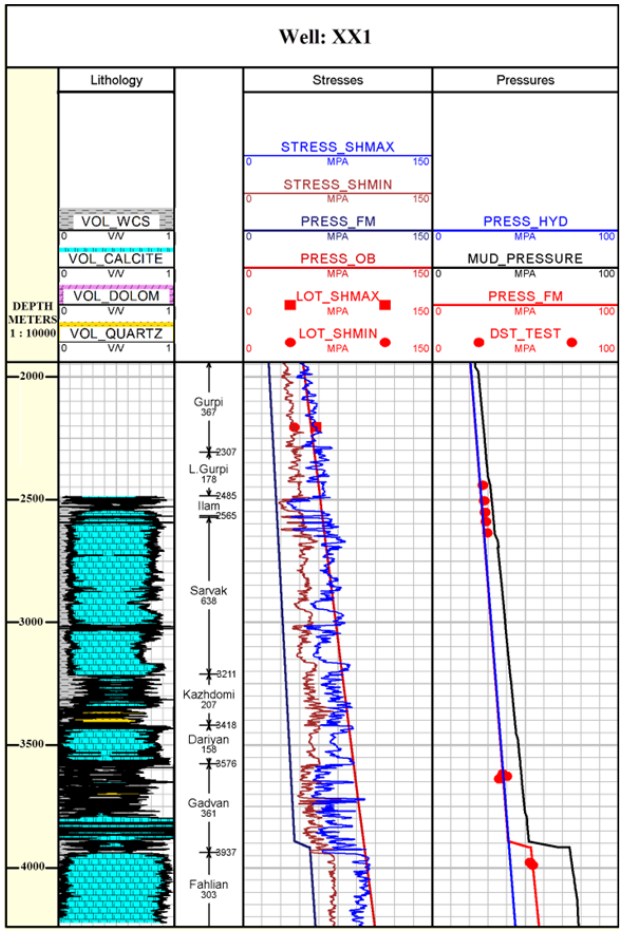

Figure 1. Stress profile for XX1 (estimated SH is based on LOT data and hydraulic fracturing theory).

Eq. (1) utilizes the density from the surface to the desired depth, where z represents the true vertical depth. However, typically, the density log is only accessible in the reservoir layers. Therefore, to calculate the vertical stress, the missing density values were substituted with the average density of the overburden layers, based on their lithology (i.e. the percentage of calcite, dolomite, etc.).

Determining the magnitude of Sh, one of the two horizontal stresses, is relatively more straightforward if it corresponds to the in-situ minimum stress (S3). By employing mini-frac and extended leak-off tests, indirect measurements of S3 (and often Sh) can be reasonably obtained. A comprehensive poro-elastic model encompasses tectonic strains and geothermal effects, thus accommodating anisotropic horizontal stresses. If the thermal terms are omitted, the model simplifies to the subsequent equations, which involve static Young's modulus E, static Poisson ratio ν, vertical total stress Sv, minimum and maximum total horizontal stresses Sh and SH, and pore pressure Pp:

$$S_h = \frac{\nu}{1-\nu}(S_V - \alpha P_p) + \alpha P_p + \frac{E}{1-\nu^2}(\varepsilon_h - \nu\varepsilon_H) \quad (2)$$

$$S_H = \frac{\nu}{1-\nu}(S_V - \alpha P_p) + \alpha P_p + \frac{E}{1-\nu^2}(\varepsilon_H - \nu\varepsilon_h) \quad (3)$$

The horizontal strains εh and εH are considered as calibration factors in this study. They are adjusted to best-match the resulting horizontal stress estimations to the available leak-off test (LOT). A leak off test data (from well XX2) was available. Figure 2 shows the LOT results in XX2 at TVD=2205m. It should be mentioned that the pressure of the mud column is added to the recorded bottomhole pressures of LOT results to present the overall pressures. A good presentation and pressure analysis for LOT is “Pressure-injection time” graphs used in Figure 2. Both leak-off point or LOP (corresponding to a distinct break-in-slope) and FBP (fracture breakdown pressure) may be easily

determined from Figure 2. The LOP can be considered approximately equal to the least principal stress [38], or the minimum horizontal stress (if not a reverse faulting regime is dominant). Therefore, the resulted LOP is interpreted as the minimum total horizontal stress which is equal to 40.66 MPa.

The "Kirsch solution" may be used to compute the initial stresses at the point of fracture. Fracture initiation (and therefore, pressure drop) takes place when the internal pressure, p, reaches its critical value, FBP. Therefore, the tangential stress σ_θ should become equal to the tensile strength σ_t. Applying this to the hydraulic fracturing test yields as a condition for creation of a hydraulic fracture and calculation of the maximum horizontal stress:

$$S_H = 3S_h - FBP + \sigma_t - P_p \quad (4)$$

The input parameters for calculating the maximum horizontal stress at 2205 m TVD are presented in Table 1. This results in a maximum horizontal stress equal to 57.69 MPa.

A pair of stress values (Sh, SH) at TVD=2205m has been obtained. These values are used to calibrate Eqs. (2) and (3) by solving the equations for the two horizontal strains εh and εH at TVD=2205m. The calibration of Eqs. (2) and (3) with the resulted maximum and minimum horizontal stresses gave horizontal strains εh and εH equal to 0.9635 and 2.7091, respectively. These horizontal strain values are used to calculate horizontal stresses in all the XX1 length. The circle and the square symbols in stress track of Figure 1 show the calculated minimum and maximum horizontal stresses obtained from LOT data and Eq. (4), respectively. According to the derived stress field in Figure 1, a normal toward strike-slip stress regime is dominated in this field. The stress regime changes to normal in lower parts of the well in Gadvan and most parts of Fahlian formations. As it will be presented in the following, the resulted stresses alongside mud pressure can accurately show the stability state of the wellbore. This in agreement with the drilling report data and wellbore diameter changes measured by a caliper. Figure 1 illustrates the stress profile for the studied well (XX1).

3.3. In situ stress orientation

Several methods for identifying stress direction are available including borehole breakout orientation, hydraulic fracture orientation, shear sonic anisotropy and dispersion and three components VSP [39].

Generally, in vertical wells and low-deviated wells, the orientation of borehole breakouts is aligned with the trend of minimum horizontal stress and drilling induced fractures are in direction of the maximum horizontal stress. However, it may not be the case with the highly deviated wells and particularly those wells that are not aligned with either of the two horizontal stresses.

The image logs are particularly useful in detecting breakouts and induced fractures. The image log was available. Borehole breakouts were observed in several sections of the well. The hole is in gauge in almost all porous zones throughout the interval. Figure 3 shows an interval of the observed breakouts.

Analysis of orthogonal calipers and their corresponding azimuthal data indicates that large majority of the borehole breakouts are elliptical in cross-section, the longer axis of which is oriented dominantly and persistently in the NW-SE direction (Figure 4). It indicates that the orientation of minimum horizontal stress (Sh) around XX1 well is almost NW-SE and the orientation of maximum horizontal stress (SH) is NE-SW. This orientation of in-situ stress is line with the orientation of regional stresses.

4. Rock strength parameter

Rock elastic properties represent the basic inputs for the estimation of rock strength and in-situ stresses, which can be later refined and calibrated to other available information.

Table 1. Input parameters to calculate SH at 2205 m TVD.

S_h (MPa)	σ_t (MPa)	FBP (MPa)	P_p (MPa)
40.66	3.22	44.46	23.055

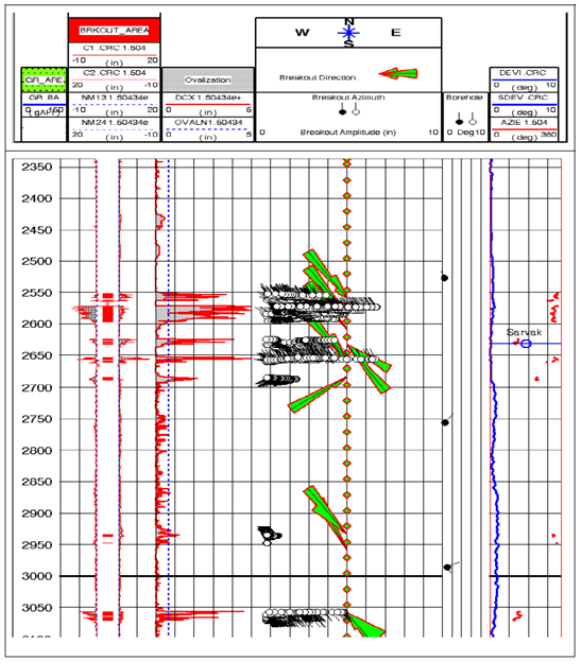

Figure 2. LOT results in XX2 at 2205m depth (pressures are bottomhole pressure).

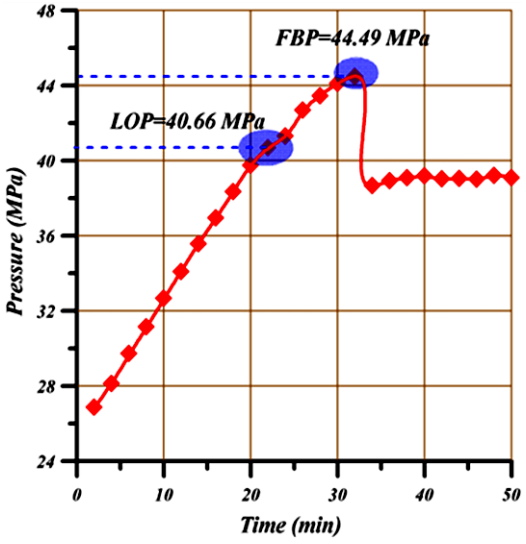

Figure 3. Breakout's direction in XX2.

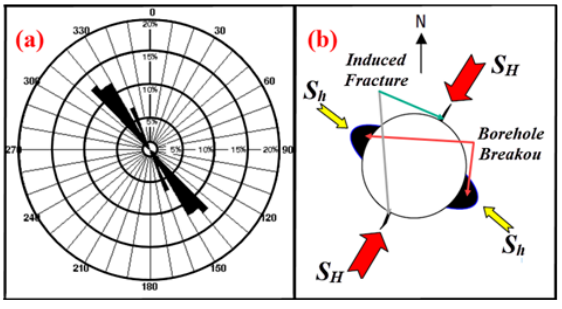

Figure 4. a) Rosette diagram of breakouts direction, b) Horizontal stresses direction in top view of XX1 with respect to the breakouts.

4.1. Dynamic strength properties

Assuming elastic isotropy and using the following equations, compressional and shear delay times and bulk density ρb from the well logs were used to calculate the dynamic elastic moduli according to Eqs. (5) to (8).

$$E_{dy} = \left(\frac{\rho}{\Delta t_P^2}\right)\left[\frac{3\Delta t_P^2 - 4\Delta t_S^2}{\Delta t_P^2 - \Delta t_S^2}\right] \quad (5)$$

$$K_{dy} = \rho\left[\frac{3\Delta t_P^2 - 4\Delta t_S^2}{3\Delta t_P^2 - \Delta t_S^2}\right] \quad (6)$$

$$G_{dy} = \left(\frac{\rho}{\Delta t_P^2}\right) \quad (7)$$

$$\nu_{dy} = \left(\frac{1}{2}\right)\left[\frac{\Delta t_P^2 - 2\Delta t_S^2}{\Delta t_P^2 - \Delta t_S^2}\right] \quad (8)$$

where, ρ is density, and Δts and Δtp are shear and compressive slowness. Shear wave delay time (DTSM) is an important parameter in calculating dynamic elastic properties. It was not available in XX1. The sonic wave data from well XX2 was used to synthesize the required DTSM for XX1.

4.1.1. Matching DTSM from well XX2

The DTSM was not available in well XX1. However, it was available in well XX2. XX2 is close to XX1 so it is assumed that they should have similar sonic logs. The compressional delay time (DT) of wells XX1 and XX2 was compared to make sure of the compatibility of their sonic data. The data were first smoothed to remove anomalous values. A code was developed to find the best matches between both well DT. The code uses an algorithm searching for the least difference (target function) of wells DTs in 50 m intervals. It is a simple least square function as follows:

$$S = \sum_{i=1}^{n} r_i^2 \, , r_i = DT_{XX1} - DT_{YY1} \quad (9)$$

DT of XX1 was considered as the base, then DT of XX2 was shifted in 50 m intervals of TVD to find the best match by minimizing Eq. (9). This led to many matched intervals, which had overlaps; these local overlapped intervals were combined resulting in the final 7 global matched intervals between XX1 and XX2. This included evaluating almost 30000 data of DT in both wells. Figure 5 shows two of the best matched data. An average value of 25 m shift-up in XX2 data was needed for the matched intervals. The matched DTs are assumed to have similar DTSM values. These DTSM intervals of XX2 were used to populate DTSM log for XX1 with the appropriate shift in the associated TVDs.

There were also some intervals that no-good match was available. In these intervals a correlation of DT and DTSM values of well XX2 was used to predict DTSM values for XX1. Eq. (10) presents the derived correlation. As it is seen both in Figure 6 and from the coefficient of determination (R2= 92.27%) a good correlation has been achieved.

$$DTSM = 145.37 - 2.71DT + 36.12 \times 10^{-3} DT^2, \mathrm{R}^2 = 92.27\% \quad (10)$$

Figure 7 (a) shows XX1 smoothed DT along with the matched smoothed DTS from XX2. The blank spots belong to the parts of data that no-good match between XX2 and XX1 was found. These parts will be populated using the derived equation (Eq. (10)). Figure 7 (b) shows the final DTS derived for XX1 well. It is a combination of the matched parts of both wells and predicted DTS using Eq. (10) for the intervals with no good match (blank parts of DTS in Figure 7 (a)). To further evaluate the robustness of the prediction, the correlation between DT and DTSM values in well XX2 (Eq. 10) was assessed using standard error metrics. The coefficient of determination (R^2=0.92) and the root-mean-square error (RMSE=7.6 μs/ft) confirm that the correlation provides a reliable estimate of shear wave slowness. For the matched intervals between XX1 and XX2, the average mismatch between compressional delay times was below 3%, which supports the assumption that the corresponding DTSM values are comparable. While these indicators do not provide full statistical confidence intervals, they serve as practical confidence bounds for the synthesized DTSM profile in XX1.

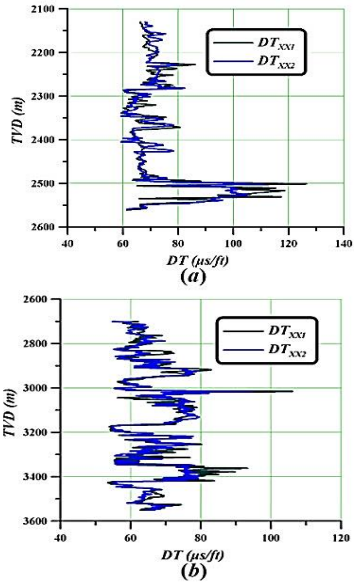

Figure 5. DT match between XX1 and XX2 (Based on XX1 TVD) a) from 2129.79 m to 2560.78 m b) from 2700.07 m to 3550.77 m (XX2 data were averagely shifted 25m up to match XX1).

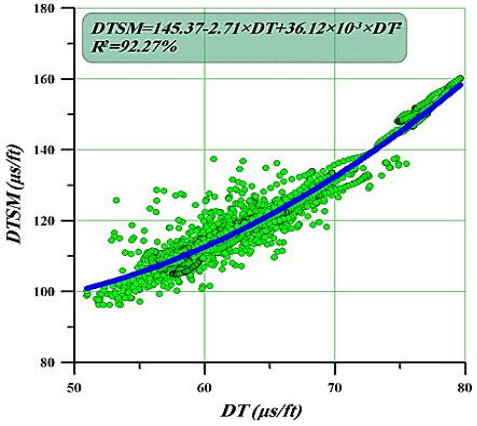

Figure 6. Correlation developed for prediction of DTSM in intervals of XX1 with no good match.

4.2. Correlations between static and dynamic properties

The dynamic properties are systematically different from the equivalent static values that are typically needed for subsequent geomechanics modeling and stress analysis. Laboratory measurements of these properties i.e. static counterparts are used to derive a correlation between dynamic and static moduli as well as Poisson's ratio. UCS, Brazilian and Triaxial tests results were used to calibrate the continuous data for UCS, tensile strength, coefficient of friction angle, cohesion and Young's modulus. As Figure 8 (a) shows there is a good correlation between Static Young's modulus from laboratory and dynamic values obtained from logs.

$$E_{Static} = 0.234E_{Dynamic} + 3.033, \quad \mathrm{R}^2 = 87.50\% \quad (11)$$

Based on the laboratory tests in this study the following correlation was used to evaluate static Poisson's ratios from dynamic log values (also see Figure 8 (b)):

$$\nu_{Static} = -0.464\nu_{Dynamic} + 0.312, \quad \mathrm{R}^2 = 88.37\% \quad (12)$$

4.3. Static strength properties

Static elastic properties were determined from rock mechanical tests on 63 core plugs, which were prepared from available core interval. Standard tests including UCS, triaxial, Brazilian, and ultrasonic tests were carried out according to ASTM.

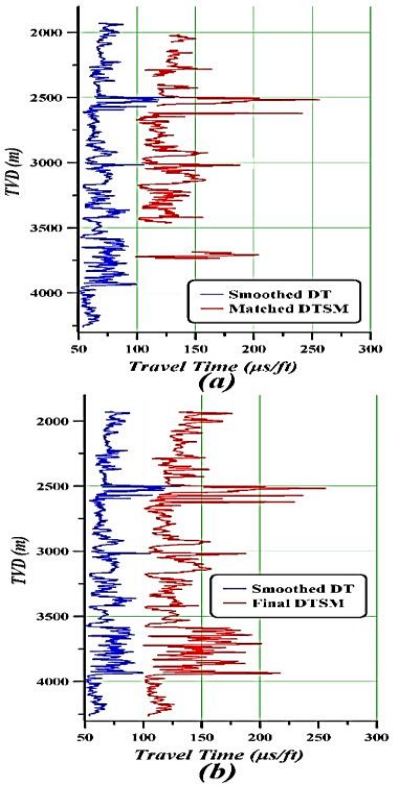

Figure 7. a) DT and matched DTSM for XX1 well, b) Final DTSM of XX1 well combining matched data and the predicted DTSM values from Eq. (2).

To enhance the understanding of the laboratory data used for calibrating dynamic to static properties, we note that the 63 core plugs subjected to UCS, triaxial, Brazilian, and ultrasonic tests were obtained from the L. Gurpi, Ilam, Gadvan, and Fahlian formations in well XX1. These formations, spanning early to late Cretaceous, encompass key lithologies (dolomite, calcite, clay, and quartz) critical to the geomechanical analysis. While precise depth intervals for these core samples are not currently available, they were selected to represent the major lithological variations across the well's producing horizons.

UCS is typically computed from log measurements. Uniaxial compressive tests or multi-stage triaxial compressive tests on whole core provide a method for point calibration of the continuous log. Several empirical equations exist for calculating UCS from log data. Most use compressive wave delay time (DT), moduli (Young's modulus and/or shear modulus), porosity and other formation properties. However, many of the published correlations are based on very limited data sets, and the most commonly used relations were largely derived from tests on rock samples from mining engineering and similar hard-rock projects, where rock strengths are usually considerably greater than those encountered in oilfield applications. Consequently, these data and log strength correlations are heavily biased toward strong rocks and away from those more porous sedimentary rocks most commonly encountered in petroleum engineering applications.

Tensile strength of the formation is used to evaluate the tensile failure of the borehole due to stress concentration. It was available from several laboratory Brazilian tests. In well XX1 there are good correlations between laboratory UCS and tensile strength with the static Young's modulus. Therefore, using the continuous profile of static Young's modulus along the well, UCS and tensile strength were calculated continuously in all the well length. The correlations are illustrated in Figure 9. It should be mentioned that UCS tests were very few (only 7 single tests in the entire well) and results contain higher uncertainty than other parameters.

$$UCS = 2.931E_{Static} - 10.122, \qquad R^2 = 89.94\% \qquad (13)$$

$$\sigma_t = 0.1542E_{Static} - 1.4426, \qquad R^2 = 80.1\% \qquad (14)$$

There were also 42 triaxial tests in various confining pressures. Young's modulus from triaxial tests are well-matched with the static log Young's modulus which is based on Eq. (11).

Figure 10 shows the various elastic properties calculated for well XX1. A good match between the static Young's modulus and also Poisson's ratio computed from the logs and the respected core sample measurements is observed. This indicates the validity of the continuous profiles of elastic properties.

Similar conclusion applies for the Poisson's ratio. The correlation of lab and field data in Figure 10, for the tensile strength and coefficient of internal friction angle have not given a fair match around 4000 m TVD. A relation based on lithology may happen to result in a better match. However, due to the lack of sufficient data, a separate relation could not be developed for different lithologies. The best possible correlation based on the available data has been presented for each parameter.

As mentioned before, DT and density are in error in several intervals (2491 m to 2593 m, 2567 m to 2575 m, 2592 m to 2595 m, 3012 m to 3031 m, 3308 m to 3315 m). The resulted cohesion and coefficient of internal friction in these intervals should not be considered correct.

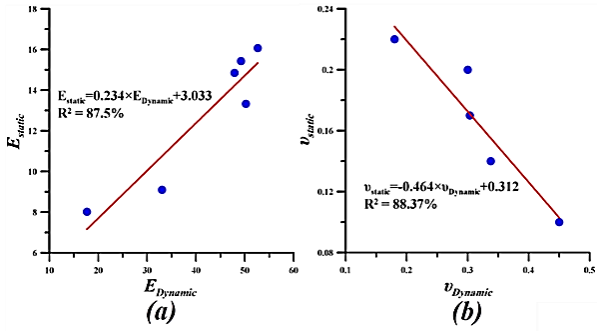

Figure 8. Correlation of dynamic and static (laboratory tests results) elastic properties in XX1, a) Young's modulus, b) Poisson's ratio.

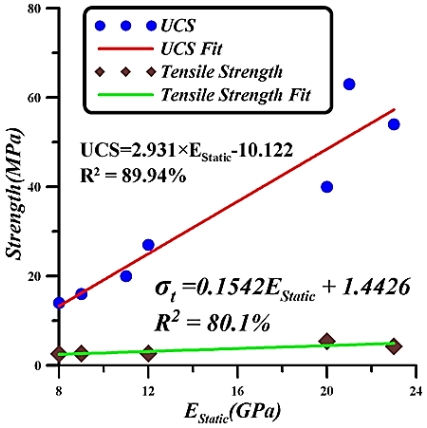

Figure 9. Correlation of UCS and Tensile strength with static Young's modulus in XX1.

5. Mud weight window

With an available MEM and the well trajectory, the stress concentrations around the borehole is calculated with the MEM as input data, and the principal stresses around the borehole can then be compared to the rock failure criteria to determine whether the borehole wall has failed or not.

Wellbore instability due to rock failure is caused by two major types of failure, tensile or shear. Shear failure or breakout is usually caused by low mud weight while induced tensile fractures are due to application

of high mud weight. Several methods exist for predicting rock failure (and wellbore instability). Mohr Coulomb criterion is widely used to determine breakouts, and maximum tensile tangential stresses are compared to tensile strength for tensile failure possibility.

One of the outputs of the wellbore stability analysis is a mud weight window. Figure 11 illustrates the concept of the mud weight window. Mud pressures less than critical breakout pressure cause pressure caving, wellbore washout, and/or kicks. Mud pressures above LOP or the minimum principal stress can re-open the natural factures/fissures, and causing loss of drilling fluid to the formation. When the mud pressure is higher than FBP, tensile failure can occur in the intact rock and hydraulic fractures will be induced in the borehole wall.

It can be seen that an ideal mud weight would be higher than the pore pressure and the minimum mud weight for preventing breakout, but lower than the minimum horizontal stress and formation breakdown pressure (both safe and stable).

The mud weight window has been computed along the trajectory of the well using the stress model and rock strength calculated for the MEM. Using the drilling reports, the applied mud weight is also added to the mud window. Applying the Mohr Coulomb failure criterion to XX1 well, shear failure and tensile failures are computed along the trajectory. Figure 12 shows a wellbore stability of XX1. From left to right tracks show Depth, Tops, Lithology, Actual caliper log data, Computed stresses, Equivalent mud window, and Pressure Window respectively.

Pressures resulting in kick, loss, breakout, and induced tensile fractures are shown in Figure 12. The black line in “mud weight” and “Pressures” tracks indicates the mud weight and mu pressure respectively. If this curve lies in any of the shaded areas, there would be a risk of kick, loss, breakout, or induced tensile fractures depending on the crossed pressure type.

The most problematic part of the well according the mud pressure used in XX1 was when the well was being drilled into Fahlian formation. Expecting high formation pressure (which is a common attribute of this formation), drill crew used a very high mud pressure in this section, causing massive mud loss. This is well predicted in Figure 12.

The interaction of mud pressure and predicted break out pressure does not fairly match with the caliper log in Gadvan formation. It is due to the uncertainty in the results of stress estimation and mechanical properties of the host rocks. The petrophysical interpretation clearly shows existence of shale in Gadvan formation. However, the available data for determination of the properties are based on the upper and lower layers with high Calcite content. This leads to overestimation of mechanical properties in Gadvan formation, which in turn underestimates the minimum required mud pressure. Therefore, the mud window has predicted a more stable condition for this formation. Decreasing the mechanical properties at this formation, which is more realistic, will produce better matching data. However, due to lack of enough data at this depth, no data manipulation has been done on the output. A brief sensitivity consideration was also carried out to evaluate the effect of data quality on the mud window prediction. In formations with incomplete or low-quality input data, such as the Gadvan interval where density and sonic logs contain errors, the derived mechanical properties may be biased toward higher values. This leads to an underestimation of the minimum required mud pressure and thus a wider predicted mud weight window. While a full quantitative uncertainty analysis is not feasible with the current dataset, we emphasize that these limitations should be taken into account when interpreting the stability results. This discussion has also been reflected in the conclusions section, where the need for additional core and log data is highlighted for more reliable predictions. Key findings in relation to the failure analysis and history matching for XX1 are the following:

- In the 12.25” hole, breakouts or/and washouts are predicted by the model across 2500-2570 m (Ilam), 3080-3109 (Sarvak) and 3580-3760 m (Gadvan). The caliper logs confirm such borehole enlargement across these zones (as seen from Figure 12),
- In the 3415-3450 interval, no drilling problems were reported in the drilling report and also model predicts no failure. It is believed that the failure visible on the caliper may have been generated when pulling out,
- In 12.25” hole, the predicted breakdown pressure is very close to the mud weight used and therefore, tripping practices should be handled with care to avoid surge and/or swabbing,
- In the 8.375” hole, the calipers show breakouts in the 3830-3880 m section (upper Fahlian), which validates the shear failure predicted by the model.
- In the 3950-TVD interval, no drilling problems were reported in the drilling report and also model predicts no failure. The caliper logs confirm such good borehole condition across these zones (as seen from Figure 12),

The mud weight used in 8.375” hole is over the mud loss pressure and therefore, lower mud weight is recommended. Also, tripping practices should be handled with care to avoid surge and/or swabbing in this section.

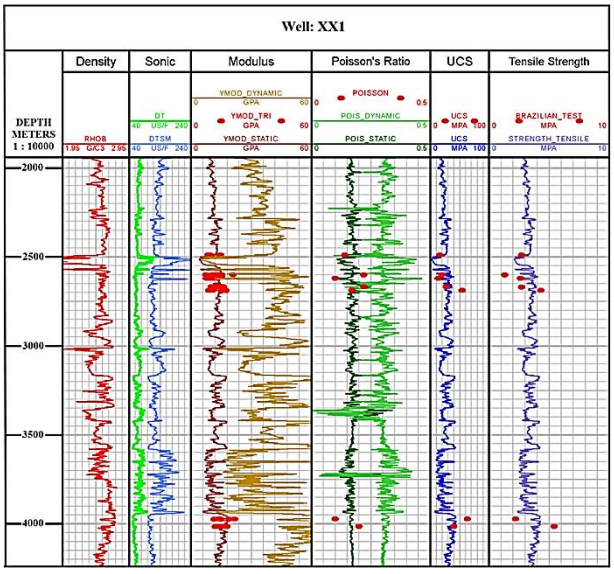

Figure 10. Continuous profile of elastic properties for XX1.

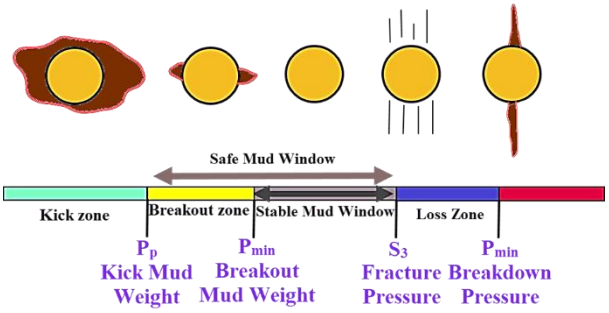

Figure 11. The mud weight window concept.

6. Wellbore trajectory sensitivity

A wellbore trajectory sensitivity analysis on the effect of the borehole deviation and drilling azimuth on the mud weight window has been performed. The wellbore trajectory sensitivity is evaluated for two depths with different stress regimes. The presented outputs result from the MEM characteristics, more precisely rock strength and stresses. Using constructed MEM for XX1, the sensitivity analysis was done in depths 2850 m (strike-slip stress regime) and 3700 m (normal stress regime) based on different deviations and azimuths. Figure 13 shows the results of the calculation of minimum and maximum mud weight pressures required for a stable drilling. The minimum mud weight pressure is calculated allowing no breakout formation. The maximum mud weight is calculated allowing no formation of induced tensile

fractures. The center of the plotted circles shows a vertical well and the well deviation will increase by going further to the outside boundary of the circles. As shown in Figure 13 (a), a vertical or a deviated well (up to 50°) in the direction of maximum horizontal stress (45° azimuth) in 2850 m TVD is the least stable well. In addition, in Figure 13 (b) a horizontal well parallel to the maximum horizontal stress (45° azimuth) in 3700 m TVD is the worst case. On the contrary, drilling parallel to the minimum horizontal stress provides the most stable trajectory. According to Figure 13, the most stable well direction is almost horizontal with a minor deviation from the minimum horizontal stress in 2850 m depth and is vertical or fairly deviated (almost 15°) in the direction of the minimum horizontal stress (135° azimuth) in 3700 m TVD. Furthermore, the required minimum mud pressure (or mud weight) decreases as deviation increases in 2850 m TVD. It means that horizontal or highly deviated wells are more stable than vertical wells. The situation is vice versa in 3700 m TVD as the required minimum mud pressure increases by increase of deviation. Therefore, vertical or moderate deviated wells are more stable than horizontal wells in this depth (mostly in Gadvan and Fahlian formations).

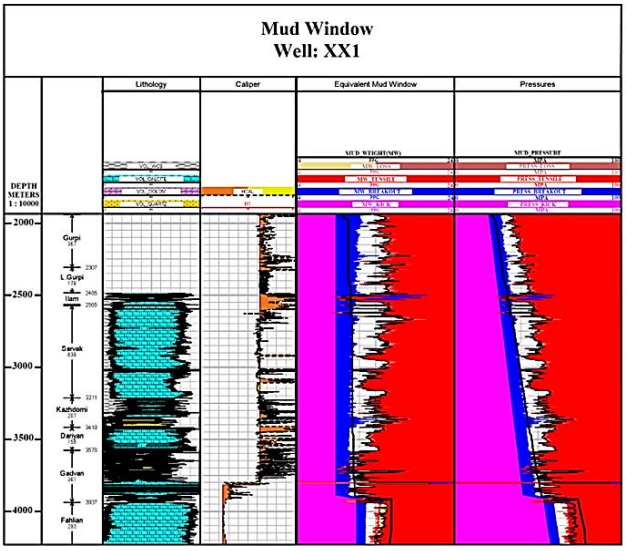

Figure 12. Wellbore stability analysis of XX1.

Figure 13 also shows the maximum mud pressure to avoid induced tensile fractures. The results for the most stable well direction is basically the same considering the maximum mud pressures. In 2850 m TVD still the horizontal well in direction of the minimum horizontal stress is the most stable direction. In 3700 m TVD a more deviated well (almost 60°) in the same direction is the most stable direction.

Since the stress field slightly changes between normal dominated stress regime and strike-slip dominated stress regime, the most stable direction also changes. Furthermore, the mud window in 3700 m (10.35 ppg-16.04 ppg) is much narrower than 2850 m (10.61 ppg-33.42 ppg) TVD. A detailed study of wellbore path is required to propose a final optimum well trajectory.

7. Conclusion

Mechanical Earth Model (MEM) for XX1 was constructed. The shear wave delay time data of adjacent well was provided. A code was developed to find the best matches of compressional delay times in XX1 and XX2. The matched intervals were assumed to have similar shear wave delay time values and intervals with no appropriate match were populated with a developed correlation. Dynamic and static elastic properties were calculated for the entire well depth. Then, pore pressure and in situ stress field was determined. A normal toward strike-slip dominated stress regime was observed in this field. Using the elastic properties and stress field, a mud window was calculated for XX1. The derived mud window alongside the mud pressure used in the well showed matching results with the drilling reports and caliper log which verifies the constructed MEM. The following results were concluded from the analysis of this well.

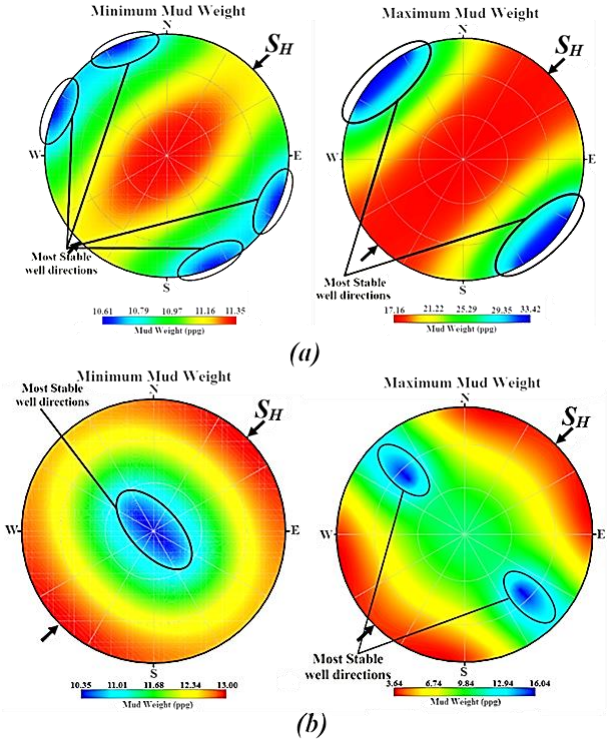

Figure 13. Sensitivity analysis of wellbore stability regarding different directions. A) at 2850 m TVD, b) at 3700 m TVD.

- The breakouts and/or washouts were detected form the MEM to be across 2500-2570 m (Ilam), 3080-3109 (Sarvak) and 3580-3760 m (Gadvan).
- Tripping practices should be handled with care to avoid surge and/or swabbing, especially in 12.25" hole.
- Breakouts occurred in 3830-3880 m section (upper Fahlian).
- The mud pressure used in Fahlian formation is over the mud loss pressure causing formation of induced tensile fractures and extensive mud loss. Therefore, a lower mud pressure in accordance with the provided mud window is recommended. Also, tripping practices should be handled with care to avoid surge and/or swabbing in this section.
- Based on the minimum and maximum required mud pressure calculations, an almost horizontal well in a direction close to the minimum horizontal stress was found to be the most stable in 2850 m TVD. Also, an average orientation of 135° (azimuth) with almost 15° deviation from vertical is recommended for the most stable wellbore in 3700 m TVD.

References

[1]. Noohnejad A, Ahangari K, Goshtasbi K. Comprehensive mechanical earth modeling using well data. Innovative Infrastructure Solutions 2021;6:1–13.

[2]. Yousefian H, Fatehi-Marji M, Soltanian H, Abdollahipour A, Pourmazaheri Y. Wellbore trajectory optimization of an Iranian oilfield based on mud pressure and failure zone. Journal of Mining and Environment 2020;11:193–220.

[3]. Abdollahipour A. Crack propagation mechanism in hydraulic

fracturing procedure in oil reservoirs. University of Yazd, 2015.

[4]. Abdollahipour A, Fatehi-Marji M, Soltanian H, Kazemzadeh EA, Marji MF, Soltanian H, et al. Behavior of a hydraulic fracture in permeable formations. Journal of Mining and Environment\ 2018;9. https://doi.org/10.22044/jme.2018.6129.1428.

[5]. Yue Y, Chen S, Wang Z, Yang X, Peng Y, Cai J, et al. Improving wellbore stability of shale by adjusting its wettability. J Pet Sci Eng 2017. https://doi.org/10.1016/j.petrol.2017.12.023.

[6]. Das B, Chatterjee R. Wellbore stability analysis and prediction of minimum mud weight for few wells in Krishna-Godavari Basin, India. International Journal of Rock Mechanics and Mining Sciences 2017;93:30–7. https://doi.org/10.1016/j.ijrmms.2016.12.018.

[7]. Mansourizadeh M, Jamshidian M, Bazargan P, Mohammadzadeh O. Wellbore stability analysis and breakout pressure prediction in vertical and deviated boreholes using failure criteria – A case study. J Pet Sci Eng 2016;145:482–92. https://doi.org/10.1016/j.petrol.2016.06.024.

[8]. De S, Varma AK, Sengupta D. Recent Advances in Well Logging Techniques for Exploration of Shale Reservoirs. Unconventional Shale Gas Exploration and Exploitation: Current Trends in Shale Gas Exploitation 2024:49–67.

[9]. Ganguli SS, Dimri VP. Reservoir characterization: State-of-the-art, key challenges and ways forward. Developments in Structural Geology and Tectonics, vol. 6, Elsevier; 2024, p. 1–35.

[10]. Li Y, Villa V, Clayton RW, Persaud P. Shear Wave Velocities in the San Gabriel and San Bernardino Basins, California. J Geophys Res Solid Earth 2023;128:e2023JB026488.

[11]. Gholami R, Moradzadeh A, Rasouli V, Hanachi J. Shear wave velocity prediction using seismic attributes and well log data. Acta Geophysica 2014;62:818–48.

[12]. Passeri F, Foti S, Rodriguez-Marek A, others. A new geostatistical model for shear wave velocity profiles. Soil Dynamics and Earthquake Engineering 2020;136:106247.

[13]. Aghakhani Emamqeysi MR, Fatehi-Marji M, Hashemizadeh A, Abolfazl Abdollahipour, Sanei M. Prediction of elastic parameters in gas reservoirs using ensemble approach. Environ Earth Sci 2023;82.

[14]. Finch WC. Abnormal pressure in antelope field North Dakota. J Petrol Technol 1969;246:821–6.

[15]. Stuart CA. Geopressures. proceedings of the 2nd symp. abnormal subsurface pressure, Baton Rouge, LA: Louisiana State Univ.; 1970.

[16]. Eaton BA. The Equation for Geopressure Prediction from Well Logs. Society of Petroleum Engineers of AIME, 1975.

[17]. Lang J, Li S, Zhang J. Wellbore stability modeling and real-time surveillance for deepwater drilling to weak bedding planes and depleted reservoirs. SPE/IADC Drilling Conference and Exhibition, Amsterdam, The Netherlands: 2011.

[18]. Bowers GL. Pore pressure estimation from velocity data; accounting for overpressure mechanisms besides undercompaction. SPE Drilling and Completions 1995:89–95.

[19]. Zhang J, Roegiers J-C. Double porosity finite element method for borehole modeling. Rock Mech Rock Eng 2005;38:217–242.

[20]. Gutierrez MA, Braunsdore NR, Couzens BA. Calibration and ranking of porepressure prediction models. The Leading Edge 2006:1516–1523.

[21]. Lopez JL, Rappold PM, Ugueto GA, Wieseneck JB, Vu K. Integrated shared earth model: 3D pore-pressure prediction and uncertainty analysis. The Leading Edge 2004:52–59.

[22]. Slotnick MM. On seismic computation with applications. Geophysics 1936;1:9–22.

[23]. Ameen MS, Smart BGD, Somerville JMC, Hammilton S, Naji NA. Predicting rock mechanical properties of carbonates from wireline logs (a case study: Arab-D reservoir, Ghawar field, Saudi Arabia). Mar Pet Geol 2009;26:430–44.

[24]. Eissa EA, Kazi A. Relation between Static and Dynamic Young's Moduli of Rocks. Rock Mechanics 1988; 25:479–82.

[25]. Marcinew M&. Fracturing of High Permeability Formations: Mechanical Properties Correlations. SPE Annual Technical Conference and Exhibition, 1993.

[26]. King MS. Static and dynamic elastic properties of rock from the Canadian Shield. Int J Rock Mech Min Sci Geomech Abstr 1983;20:237–41.

[27]. Lacy LL. Dynamic rock mechanics testing for optimized fracture designs. SPE Annual Technical Conference and Exhibition, San Antonio, TX: Society of Petroleum Engineers.; 1997.

[28]. Wang Z. Dynamic vs. Static Elastic Properties of Reservoir Rocks, in Seismic and acoustic velocities. reservoir rocks, Society of Exploration Geophysicists; 2000.

[29]. Bradford IDR, Fuller J, Thompson PJ, Walsgrove TR. Benefits of Assessing the Solids Production Risk in a North Sea Reservoir Using Elastoplastic Modelling. SPE/ISRM Rock Mechanics in Petroleum Engineering, Trondheim, Norway: 1998.

[30]. McNally GH. The prediction of geotechnical rock properties from sonic and neutron logs. Geophys Explor 1990;21:65–71.

[31]. Moos D, Zoback MD, Bailey L. Feasibility study of the stability of openhole multilaterals. SPE Mid- Continent Operations Symposium, Oklahoma City, Oklahoma: 1999.

[32]. Kazi A, Zekai S, Bahsa-Eldin H. Relationship Between Sonic Pulse Velocity and Uniaxial Compressive Strengths of Rocks. Proc. of the 24th U.S. Symp. on Rock Mech., Texas A&M University; 1983.

[33]. Nygaard R, Hareland G. Application of rock strength in drilling evaluation. SPE Annual Technical, 2007.

[34]. Asef MR, Farrokhrouz M. Governing Parameters for Approximation of Carbonates UCS. EJGE 2010;15.

[35]. Jaeger JC, Cook NGW. Fundamentals of Rock Mechanics. New York: Chapman and Hall; 1979.

[36]. Zoback M, Mooss D, Mastin L, Anderson R. Wellbore breakout and in situ stress. J Geophys Res 1985;90:5523–5530.

[37]. Zoback MD, Mastin L, Barton C. In situ stress measurements in deep boreholes using hydraulic fracturing, wellbore breakouts and Stonely wave polarization. ISRM International Symposium, Stockholm, Sweden: International Society for Rock Mechanics and Rock Engineering; 1986.

[38]. Zoback MD, Barton CA, Brudy M, Castillo DA, Finkbeiner T, Grollimundb BR, et al. Determination of stress orientation and magnitude in deep wells. International Journal of Rock Mechanics & Mining Sciences 2003;40:1049–76.

[39]. Perdona P, C. Rabe. Laboratory test and logging campaign for geomechanical application in SAGD process for heavy oil reservoirs in Venezuela. In: Zhao J, Labiouse V, Dudt J-P, Mathier J-F, editors. EUROCK 2010:, 2010, p. 737–40.